



Original Article

Land Surface Temperature Correlation with Land use Land cover through Landsat Data in Solapur District

Swapnil Kalpavruksha¹, Anil Yedage²

^{1,2} School of Earth Sciences, Panyashlok Ahilyadevi Holkar Solapur University Solapur-Pune National Highway, Kegaon, Solapur- (Maharashtra) (India)

Manuscript ID:
RIGJAAR-2025-0201010

ISSN: 2998-4459

Volume 2

Issue 1

Pp. 36-45

January 2025

Submitted: 28 Nov 2024

Revised: 18 Dec 2024

Accepted: 25 Jan 2025

Published: 31 Jan 2025

Correspondence Address:

Swapnil Kalpavruksha, School of Earth Sciences, Panyashlok Ahilyadevi Holkar Solapur University, Solapur-Pune National Highway, Kegaon, Solapur- (Maharashtra) (India)
Email: anilyedage@gmail.com

Quick Response Code:



Web: <https://rlgjaar.com>



DOI: 10.5281/zenodo.15553227

DOI Link:

<https://doi.org/10.5281/zenodo.15553227>



Creative Commons



Abstract

Land Surface Temperature (LST) is a pivotal element in understanding land surface processes and serves as a vital metric for assessing the impacts of climate change. Vegetation identification through remote sensing is enabled by the distinct absorption characteristics of vegetation in the red and blue bands of the visible spectrum, along with fluctuations in green reflectance, and a particularly strong reflectance in the near-infrared (NIR) region. In this study, the focus area is Solapur district, Maharashtra. Multi-temporal satellite imagery from Landsat 8, specifically for the years 2014 and 2024, was utilized to retrieve and analyze LST values. The analysis was conducted using QGIS software. The highest LST recorded in 2024 was 48.50218 °C, with the lowest at 28.5021 °C. In comparison, the year 2014 showed a maximum LST of 45.055 °C and a minimum of 24.0892 °C. LST is a critical variable for comprehending surface energy balance and climate dynamics, especially in urban and semi-arid regions. The study employs Landsat 8 Thermal Infrared Sensor (TIRS) and optical reflectance data to calculate LST using a standardized workflow involving radiometric calibration, atmospheric correction, and land surface emissivity estimation. Vegetation indices such as the Normalized Difference Vegetation Index (NDVI) were used to determine emissivity and explore the relationship between LST and different land cover classes. The results indicate significant spatial and temporal variations in LST, highlighting the presence of urban heat island (UHI) effects and notable land use/land cover (LULC) changes over the decade. This research demonstrates the effectiveness of remote sensing and GIS technologies in monitoring urban thermal environments and provides valuable insights for sustainable urban planning in rapidly growing cities like Solapur.

Keywords: QGIS, Land Surface Temperature (LST), Land Use/Land Cover (LULC) and Urban Heat Island (UHI)

Introduction

The phenomenon known as Urban Heat Island (UHI) transpires when the temperature within urban locales exceeds that of adjacent rural environments [1]. This occurrence is partially attributable to heat that is emitted, retained, or re-radiated from anthropogenic thermal sources present within the urban matrix [2]. Conversely, Urban Cool Islands (UCIs) are frequently observed in urban environments, particularly within arid and semi-arid regions, where irrigated or verdant surfaces engender "cool islands" or an "oasis" effect [3] amidst urban landscapes. UCIs are, to a certain extent, ascribed to the processes of evapotranspiration from moist surfaces and transpiration from foliar structures, wherein the radiant energy that influences the surface energy equilibrium is transformed into latent heat [4]. This transformation leads to the emergence of "cool islands" that exhibit temperatures ranging from 2.5 to 6 °C lower in comparison to their immediate surroundings [5], predominantly during daylight hours [6,7]. Both UHI and UCI exert profound influences on various domains including the atmosphere, ecology, environment, economy, society, and public health [8]. A comprehensive understanding of the spatial distributions and characteristics of UHIs and UCIs is essential for urban or regional planning endeavors aimed at enhancing the well-being of citizens, for instance, through the establishment of parks and green belts in hot and arid locales [9]. Numerous factors contribute to the magnitude of UHIs and UCIs.

Creative Commons (CC BY-NC-SA 4.0)

This is an open access journal, and articles are distributed under the terms of the Creative Commons Attribution-NonCommercial-ShareAlike 4.0 International Public License, which allows others to remix, tweak, and build upon the work noncommercially, as long as appropriate credit is given and the new creations are licensed under the identical terms.

How to cite this article:

Kalpavruksha, S., & Yedage, A. (2025). Land Surface Temperature Correlation with Land use Land cover through Landsat Data in Solapur District. Royal International Global Journal of Advance and Applied Research, 2(1), 36–45. <https://doi.org/10.5281/zenodo.15553227>

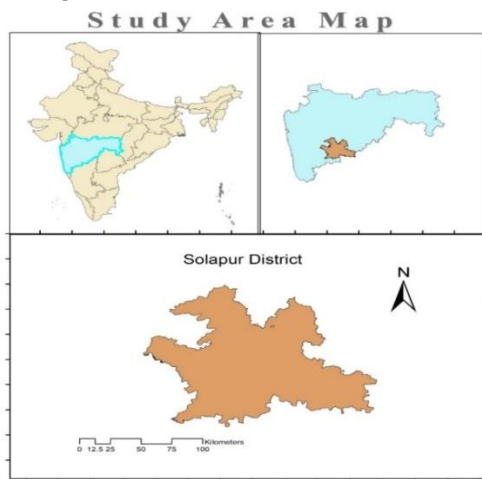
For instance, the surface albedo is instrumental in facilitating the formation of cooler "islands" [10], while the reflectance and roughness attributes of land use and land cover (LULC) [11,12], as well as the configuration, complexity, intensity [13–17], Morphology, and heterogeneity [18] of terrestrial objects, including edifices and their constituent materials [19] and elevations [20], significantly influence the intensity of the UHI effect. Generally, urban artificial impervious surfaces (e.g., asphalt thoroughfares and residential, commercial, and industrial land uses) are frequently distinguished by elevated land surface temperatures (LSTs) in comparison to natural LULC types such as aquatic bodies, urban parks, and green spaces [17–19,21]. Additionally, microclimatic factors, encompassing wind velocity and cloud coverage, also play a

pivotal role in modulating the intensity of the UHI phenomenon [22] in this study region rural area most of cover in sugarcane crop and horticulture crops.

Study Area

Solapur city is situated in the southeastern quadrant of Maharashtra, India, positioned at coordinates 17.6599° N latitude and 75.9064° E longitude. It represents one of the key urban centres within the state, fig.1 showcasing a distinctive amalgamation of industrial, agricultural, and residential land utilization. The urban expanse of the city encompasses an estimated area of 178.57 square kilometres and has undergone substantial urban expansion in the preceding decades.

Figure.1



This investigation is focused on the urban locality of Solapur, situated in the state of Maharashtra, India. Solapur occupies a position in the southwestern quadrant of Maharashtra and is located at an elevation of approximately 457 meters above sea level, characterized by a semi-arid climate that features elevated summer temperatures and temperate winter conditions. The city serves as a significant economic and industrial nucleus within the region, with its predominant sectors encompassing textiles, sugar production, and agricultural activities. The economic potential and strategic geographical placement of Solapur have contributed to its rapid demographic expansion and urban development over recent decades.

Solapur is positioned within a semi-arid environment, rendering it particularly vulnerable to thermal stress. The climatic profile of Solapur is marked by elevated temperatures, minimal precipitation, and prolonged dry periods. These environmental conditions confer a distinctive susceptibility to heat stress upon the city, as urban surfaces typically absorb and retain heat, resulting in elevated temperatures and exacerbating the Urban Heat Island (UHI) phenomenon. The lack of vegetative cover and limited water resources further exacerbate this challenge, underscoring the necessity to understand and mitigate the impacts of rising temperatures on both the ecosystem and inhabitants of the urban area. By investigating Land Surface

Temperature (LST) variations in Solapur, scholars can derive critical insights into the unique challenges presented by the semi-arid climate and formulate targeted strategies aimed at enhancing resilience and promoting adaptation.

Solapur is characterized by rapid urban expansion, accompanied by significant alterations in land use and land cover. The economic prospects and strategic positioning of Solapur have facilitated its accelerated growth in terms of population and urbanization in recent decades. As the city expands, natural landscapes are being converted into constructed environments, leading to substantial changes in land use and land cover. The conversion of permeable surfaces into impervious infrastructures, such as roads, edifices, and parking facilities, is altering the thermal properties of the land surface and intensifying the emergence of the UHI effect. A comprehensive understanding of the dynamics of Land Use and Land Cover (LULC) change in Solapur is essential to assess their effects on LST and to devise sustainable urban planning strategies that mitigate detrimental environmental consequences.

The region is characterized by predominantly flat to gently undulating topography, agricultural territories, open spaces, sparse vegetation, and an encroaching urban landscape. Given its climatic sensitivity and ongoing urbanization, Solapur presents an ideal case study to examine trends in Land Surface Temperature (LST) and the

temporal changes in land use and vegetative patterns. This research site was selected not solely for its pronounced urban growth but also for its ecological significance in the context of evaluating sustainable urban development and planning methodologies amid the challenges posed by climate change.

Materials and Methods:

Estimating Land Surface Temperature (LST) The remotely sensed data, meticulously gathered by the Landsat series of satellites—including various models such as Landsat 5, 7, and 8—prove to be particularly beneficial for the estimation of Land Surface Temperature (LST). This advantage is primarily attributed to the incorporation of thermal infrared radiometers that are adeptly integrated into the onboard systems of these satellites, thus rendering the data they acquire highly appropriate for LST estimations that can be effectively employed in applications such as the characterization of Urban Heat Islands (UHI). In the purview of this complex research initiative, we systematically derived our estimations of Land Surface Temperature (LST) from Band 10, which is associated with Thermal Infrared (TIR₁) data that underwent resampling from its original spatial resolution of 100 meters to a more refined resolution of 30 meters, encapsulating the spectral range of 10.60–11.19 μm , all of which were procured from the extensive observations conducted by Landsat-8 (for a comprehensive and detailed elucidation of the employed methodology, please consult Appendix A). The in-situ measurements that were rigorously executed transpired within the temporal interval extending from 2014 to 2024; however, it is noteworthy that during the entirety of these specified dates, there were regrettably no recorded overpasses of the Landsat-8 satellite over the designated Area of Interest (AOI).

In accordance with our research aims, we subsequently utilized a total of four distinct Landsat-8 satellite overpasses, which proficiently captured imagery that was temporally proximate to the exact moments when the in-situ measurements were scrupulously gathered, specifically on the dates within the years 2014 to 2024. To facilitate a meticulous analysis regarding the correlation between Land Surface Temperature (LST) and Land Use/Land Cover (LULC), we executed the calculation of median Land Surface Temperature values derived from these previously mentioned four Landsat-8 overpasses, occurring on the dates in the year 2024. To enable a comprehensive and direct comparison with both in situ data and the estimates derived from Potential Evapotranspiration (PET), which were compiled over the span of time, it was deemed imperative to ensure a high degree of temporal accuracy, particularly concerning potential variations in meteorological conditions; hence, we computed the mean Land Surface Temperature from the Landsat-8 overpass that occurred immediately prior to the in situ collection date (on 04 April 2014) as well as the mean from the subsequent overpass that took place immediately following the in situ collection dates (on 15 April 2024).

The overall downloaded Landsat 8 imagery exhibited cloud cover percentages of 9% and 16% for the

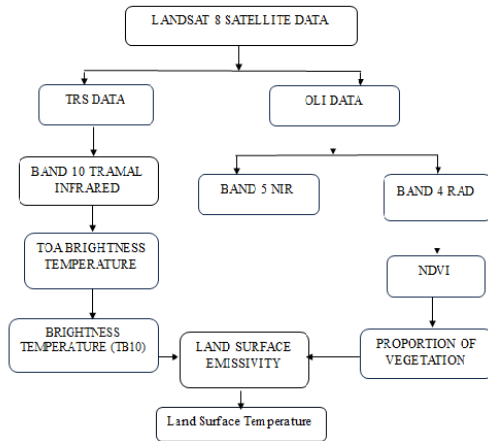
Row-Path of 150/36 and 150/37, flowchart .1 respectively; however, the study area demonstrated an absence of cloud cover. The acquired Landsat 8 (OLI/TIRS) data is accessible on the USGS website in a geometrically corrected format, and as such, no geometric correction was necessitated.

Radiative Transfer Model

Remote sensing facilitates the detection of electromagnetic radiation (EMR) from various terrestrial objects utilizing sensors affixed to a remote sensing platform, thereby enabling the analysis of the spectral response associated with land surface characteristics [29]. The wavelength spectrum for LST measurements within the EMR domain predominantly resides in the thermal infrared (TIR) range, spanning from 8 to 15 μm [1]. TIR-based sensors capture EMR in Top of Atmosphere (TOA) radiances [30]. During diurnal periods, there exists both emission and reflection of EMR; conversely, the sensed EMR during nocturnal periods is confined solely to emission. The inverse of Planck's law is employed to derive blackbody/brightness temperatures from TOA radiances, which can subsequently be corrected and converted to LST [31]. Numerous methodologies [1] are available for this purpose [32, 33]. Vegetation indices, such as NDVI, measure fluctuations in terrestrial vegetation due to their capacity to absorb photosynthetically active radiation [21, 34, 35]. The NDVI data is procured from various satellites, including MODIS, Landsat, and AVHRR [36]. In the present investigation, the estimation of LST was conducted utilizing a single-channel algorithm-based radiative transfer model [37, 38]. The radiative transfer model constitutes the foundation of LST inversion theory, which is instrumental in estimating LST from remote sensing satellite data [39]. A plethora of studies has demonstrated that employing a radiative transfer model to estimate LST from satellite remote sensing thermal data yields greater accuracy than utilizing a universal single-channel algorithm [40]. The current research employed a radiative transfer model to estimate LST from Landsat 8 TIRS data. The estimation of LST in this study encompassed satellite data pre-processing (radiation calibration), the calculation of radiance for TIRS band 10, atmospheric correction, NDVI and emissivity calculations, the radiance computation for a black body at the equivalent temperature, and the estimation of LST [41].

Where $L_{\text{sensor},i}$ is the sensor's thermal infrared radiance for the i th band, and ϵ_i is the sensor's land surface specific emissivity for the i band ($\text{W}/(\text{m}^2 \text{sr m})$). $B_i(T_s)$ represents the Planck black body thermal radiance ($\text{W}/(\text{m}^2 \text{sr m})$), where T_s is the LST in Kelvin (K). From the ground the total atmospheric transmittance to the sensor in band i is denoted by τ_i where Latm,i represents downward radiation and Latm,i represents upward radiation ($\text{W}/(\text{m}^2 \text{sr m})$). The NASA's website (<https://atmcorr.gsfc.nasa.gov/>), were used for atmospheric parameters and Latm,i , and Latm,i were calculated using the imaging time, latitude, and longitude.

Flowchart 1



$$L\lambda = ML * Qcal + AL$$

Where:

$L\lambda$ = Top of Atmosphere (TOA) spectral radiance (Watts/ (m² * sr * μm))

ML = Radiance multiplicative band (No.)

AL = Radiance additive band (No.)

Qcal = Quantized and calibrated standard product pixel values (DN)

In this context, Bi (Ts) represents the black body radiance value within the thermal infrared spectrum, whereas K1 and K2 were derived from the image header file. The specific values for K1 and K2 were identified as 774.89 W/m² sr μm and 1321.08 W/m² sr μm, respectively [32].

$$BT = K2 / \ln(K1 / L\lambda + 1) - 272.15$$

Where:

BT = Top of Atmosphere brightness temperature (°C)

$L\lambda$ = TOA spectral radiance (Watts/ (m² * sr * μm))

K1 = K1 constant band (No.)

K2 = K2 constant band (No.)

Normalized difference vegetation index (NDVI)

The disparities in near-infrared and red reflectance of green vegetation were employed to ascertain the NDVI, which exhibited a range from -1 to 1.

The NDVI was computed by employing the subsequent formula outlined in (equation (6)) [32]:

$$NDVI = (NIR - RED) / (NIR + RED)$$

Where:

RED = DN values corresponding to the RED band

NIR = DN values corresponding to the Near-Infrared band

Herein, ρ_4 designates the reflectance of the red band (0.64–0.67 μm) and ρ_5 represents the reflectance of the near-infrared band (0.85–0.88 μm).

NDVI was utilized to derive surface emissivity employing the mixed image separation methodology [32,42]. However, surfaces exhibiting emissivity values below 0.85 are predominantly identified in desert environments. In contrast to the emissivity of aquatic bodies such as oceans, the emissivity of terrestrial surfaces may vary significantly across different locations [30].

$$PV = [(NDVI - NDVI \min) / (NDVI \max + NDVI \min)]^2$$

Where:

PV = Proportion of vegetation

NDVI = DN values derived from the NDVI image

NDVI min = Minimum DN values derived from the NDVI image

NDVI max = Maximum DN values derived from the NDVI image

Emissivity may vary in response to the viewing angle, surface moisture content, and roughness, as well as vegetation cover. Although multiple methodologies exist for the calculation of emissivity, the mixed separation method was selected due to the presence of diverse land use and land cover (LULC) types within the study area [43].

$$E = 0.004 * PV + 0.986$$

Where:

E = Land surface emissivity

PV = Proportion of vegetation

The land surface was initially categorized into water bodies, built-up areas, and natural surfaces. The water body was assigned an emissivity value of 0.995. In this study, NDVI denotes the Normalized Difference Vegetation Index, with (NDVI)_v and (NDVI)_s representing the NDVI values for vegetation and bare soil, respectively. In the present analysis, PV was approximated by assigning (NDVI)_v and (NDVI)_s values of 0.7 and 0.05, correspondingly, as the pixels within the study area did not exhibit clear delineation of complete bare soil or vegetation coverage. The PV value was determined to be 1 when the NDVI of a pixel surpassed 0.70, and 0 when it fell below 0.05; thus, when the NDVI of a pixel exceeded 0.70, it was deemed to be entirely covered by vegetation. Conversely, the pixel was classified as being completely covered by bare soil when its value was less than 0.05. Upon estimating emissivity, Land Surface Temperature (LST) was calculated utilizing equations (50). $LST = (BT / 1) + W * (BT / 14380) * \ln(E)$

Where:

BT = Top of atmosphere brightness temperature (°C)

W = Wavelength of emitted radiance

E = Land surface emissivity

Land use land cover types

The LULC maps were generated utilizing the Maximum Likelihood Classification (MLC) technique,

predicated on the probability of user-provided training samples [44]. The LULC types within the study area were classified into built-up regions, bare soil, agricultural land, vegetation, and water bodies. The precision of LULC classification was evaluated using 40 ground truth points collected from each LULC class during field surveys. To enhance the accuracy of LULC classification, ground control points, spectral and spatial profiles, and supplementary information from Google Earth images were employed to develop training samples. The confusion matrix method, which is widely applied for assessing the accuracy of LULC classification, was utilized to evaluate the classification accuracy [45].

Association Between LST, NDVI, and Aspect

A comprehensive understanding of the complex interrelationship that exists between Land Surface Temperature (LST) and the Normalized Difference Vegetation Index (NDVI) is essential. which functions as a critical metric or surrogate for evaluating both the density and overall vitality of flora within a specified region, has been utilized for analytical endeavors. Typically, it is observed that heightened NDVI values, which denote the existence of dense and flourishing vegetation, correlate with diminished land surface temperatures as a consequence of the processes of evapotranspiration and the shading effects imparted by such vegetation, whereas reduced NDVI values, which are representative of bare soil or significantly developed urban environments, generally exhibit elevated land surface temperatures.

The concept of "aspect," which relates to the specific compass direction that a slope or hillside is oriented towards, assumes a pivotal role in determining the quantity of solar radiation that a specific area receives throughout the diurnal cycle:

In the northern hemisphere, slopes oriented towards the south and southwest tend to be subjected to a greater extent of direct solar radiation, which subsequently contributes to the emergence of elevated surface temperatures in those locales. In contrast, slopes directed towards the north typically undergo cooler temperature conditions as a direct result of their diminished exposure to solar radiation, leading to lower land surface temperature values when juxtaposed against their sun-exposed counterparts. The extensive analysis performed revealed a significant negative correlation between NDVI and LST, thereby substantiating the hypothesis that vegetation cover exerts a substantial moderating influence on surface temperatures. Conversely, the aspect of the terrain was determined to affect variations in land surface temperature, with higher temperature values being documented on slopes that are more exposed to sunlight and lower temperature values being recorded on slopes that are predominantly shaded. This specific spatial trend became increasingly pronounced in regions characterized by heterogeneous topographical features located on the periphery of Solapur city.

Spatial Distribution of LST and NDVI

Utilizing the capabilities of QGIS in conjunction with Landsat 8 satellite data acquired for the years 2014 and 2024, comprehensive spatial distribution maps were meticulously constructed for both land surface temperature (LST) and the normalized difference vegetation index (NDVI). The principal findings of this analysis encompass:

LST Distribution:

It was predominantly discerned that elevated values of land surface temperature were primarily concentrated within urban centers, industrial districts, and areas exhibiting sparse vegetation cover.

The northern and central sectors of Solapur manifested the most pronounced increments in temperature levels when comparing data from the years 2014 and 2024, underscoring significant alterations in thermal conditions.

NDVI Distribution:

The allocation of higher NDVI values was notably concentrated in areas characterized by agricultural practices, green spaces, and riverine zones located around the city's periphery, signifying healthier vegetation in those regions. A significant reduction in NDVI values was observed in areas undergoing rapid urbanization, which serves as an indicator of vegetation loss attributable to modifications in land cover associated with developmental activities. The overlay analysis performed between the Normalized Difference Vegetation Index (NDVI) and Land Surface Temperature (LST) maps provided a definitive demonstration that regions characterized by substantial vegetation correlate with markedly lower surface temperatures, thereby underscoring the essential cooling influence that green coverage exerts in alleviating the repercussions of the Urban Heat Island (UHI) phenomenon, particularly within the specific milieu of Solapur.

Results

The exhaustive examination undertaken on the Land Surface Temperature (LST) within the geographical parameters of Solapur city over an extensive temporal span of ten years, which utilized the sophisticated functionalities of Landsat 8 imagery corresponding to the years 2014 and 2024, has revealed significant and remarkable spatial and temporal variations, which are emblematic of both natural environmental determinants and anthropogenic endeavors that profoundly affect the urban thermal environment.

LST Variation in 2014 and 2024

2014: Maximum LST: 45.055 °C **Minimum LST:** 24.0892 °C The average Land Surface Temperature documented in the year 2014 was determined to be relatively moderate, with the elevated temperature zones predominantly located within the central urban locales and along the essential transit routes that facilitate mobility within the city. fig:2

Figure 2

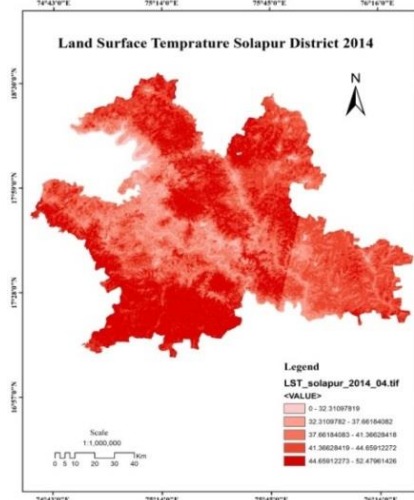
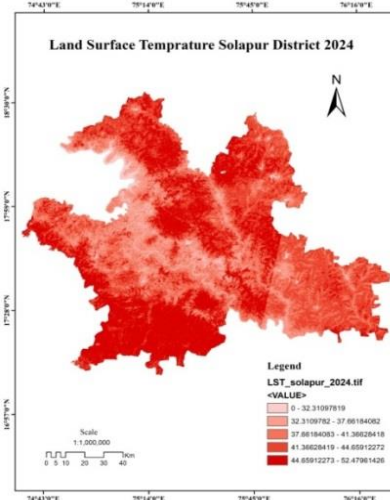


Figure 3



2024: Maximum LST: 48.50218 °C **Minimum LST:** 28.5021 °C A distinct and discernible escalation in both the maximum and minimum Land Surface Temperature values was recorded in the year 2024, fig.3 which serves to signify a substantial intensification of surface heating. The

Spatial Distribution and Urban Heat Island Effect

The Land Surface Temperature maps that were meticulously constructed utilizing QGIS for both years under scrutiny indicate that: Urbanized and developed areas consistently exhibited elevated Land Surface Temperature values as a direct consequence of the materials utilized in construction, such as asphalt and concrete, in conjunction with a notable diminishment in the overall vegetation cover that would otherwise facilitate temperature regulation.

Peripheral and green zones, inclusive of agricultural lands and open spaces, exhibited a comparatively lower range of Land Surface Temperature values, thereby reinforcing the divergent thermal characteristics between urbanized and non-urbanized regions. In the year 2024, the spatial extent of the high-LST zones, defined as those exceeding 40 °C, expanded considerably, encroaching into regions that were previously characterized by vegetation or remained undeveloped, thereby corroborating the intensification of the Urban Heat Island (UHI) phenomenon that is increasingly manifest in urban settings.

NDVI and Emissivity Relationship

The emissivity estimates derived from the Normalized Difference Vegetation Index (NDVI) illustrated an inverse correlation with Land Surface Temperature: Elevated NDVI values, indicative of substantial vegetation presence, were associated with lower Land Surface Temperature measurements, which serves to validate the

proliferation of high-temperature zones within the urban fabric indicates a direct association with the ongoing dynamics of urbanization and an augmentation in the extent of impermeable surfaces that typify such developments.

cooling influence that vegetation exerts on its immediate environment. Conversely, areas characterized by diminished NDVI values, which typically encompass urban or barren terrains, exhibited significantly elevated Land Surface Temperature values, thereby reinforcing the pronounced effect that diverse land cover types exert on surface temperature dynamics.

Temporal Comparison and LULC Impact

In the evaluative examination undertaken between the years 2014 and 2024, a discernible escalation in the high Land Surface Temperature (LST) zones was documented, as demonstrated by a substantial increase in both the quantity and area of pixels that reported Land Surface Temperatures surpassing 45 °C, thereby highlighting a troubling trajectory in surface thermal elevation. Furthermore, a significant diminution in areas characterized by greenery and low-LST was noted, with locales that were formerly rich in dense flora or aquatic bodies undergoing fragmentation or a reduction in coverage as a consequence of the incessant proliferation of urban sprawl emblematic of contemporary developmental paradigms. The data subjected to analysis indicate a profound metamorphosis in Land Use/Land Cover (LULC), fig.4 and fig.5 particularly emphasizing the transformation of agricultural and fallow lands into residential, commercial, and industrial districts, which bears substantial ramifications for urban ecology and environmental integrity.

Figure 4

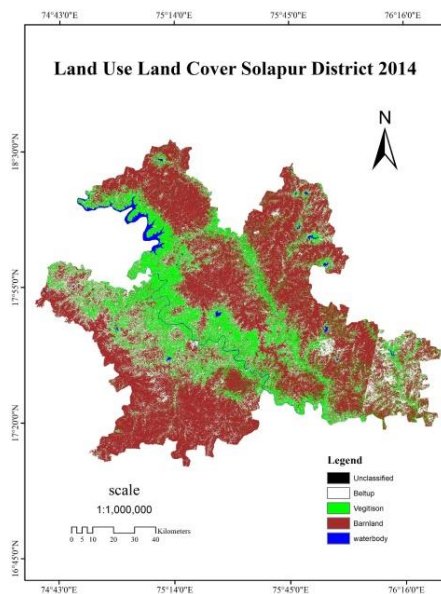
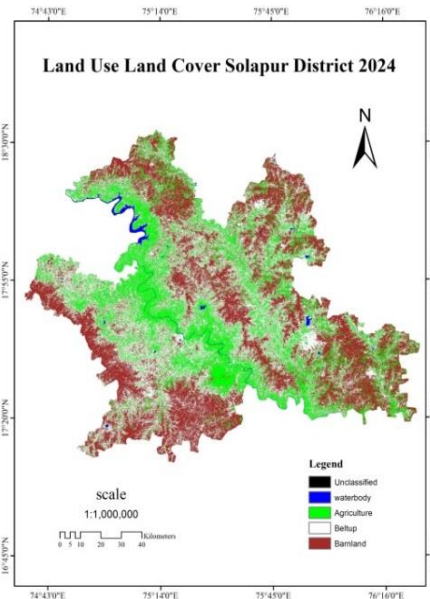


Figure 5



Zonal Statistics and Classification

An exhaustive zonal statistical evaluation, which utilized the administrative or ward boundaries that delineate Solapur, elucidated that the central urban zones exhibited the highest average Land Surface Temperatures across both analysed years, thereby signifying a sustained pattern of thermal concentration within urban nuclei. Notably, the recently urbanized peripheral areas, which were relatively cooler in the year 2014, now exhibit heightened Land Surface Temperatures in the year 2024, thereby underscoring the fluid dynamics of urban temperature distributions. The most pronounced acceleration in temperature augmentation was recorded in transitional zones, which accentuates the thermal ramifications associated with rapid urbanization and underscores the imperative for strategic urban planning aimed at alleviating adverse impacts.

Implications for Urban Planning

The documented escalation in Land Surface Temperature alongside the corresponding proliferation of Urban Heat Island phenomena accentuates the urgent need for: The execution of urban greening initiatives, such as the establishment of arboreal cover and the creation of recreational parks, which can significantly contribute to the alleviation of urban heat. Moreover, the integration of reflective or vegetative roofing methodologies within construction practices is critical to augment thermal efficiency and diminish heat retention in metropolitan areas. In addition, the formulation of zoning policies aimed at regulating heat-generating developments is crucial to guarantee sustainable urban advancement. These findings collectively furnish a substantial empirical basis for the development of sustainable urban planning methodologies, the creation of climate-resilient infrastructures, and the formulation of effective environmental policies tailored to the unique context of Solapur.

Conclusions

The current academic inquiry was meticulously structured with the principal aim of extracting and comprehensively scrutinizing the Land Surface Temperature (LST) specifically within the geographical boundaries of Solapur city, situated in the state of Maharashtra, through the implementation of a robust methodology that incorporates multi-temporal satellite data procured from the Landsat 8 satellite across the temporal spectrum of 2014 to 2024. The strategic deployment of sophisticated Remote Sensing (RS) techniques, in conjunction with Geographic Information System (GIS) tools, enabled the accurate quantification and intricate spatial examination of not only LST but also the Normalized Difference Vegetation Index (NDVI) alongside notable transformations in land use and land cover (LULC). The findings of this comprehensive research elucidate that Solapur has experienced a significant and statistically demonstrable escalation in LST over the last decade, as substantiated by the recorded peak surface temperatures which have surged from a noteworthy 45.05 °C in 2014 to an even more concerning 48.50 °C in 2024. This substantial increase in temperature is intricately linked to considerable urban proliferation coupled with a marked reduction in the extent of vegetative cover, thus providing a clear and compelling representation of the Urban Heat Island (UHI) effect that is prevalent in urbanized locales. By employing NDVI-based estimation methodologies for the determination of emissivity values alongside thorough LULC classification, this research has adeptly discerned a robust and statistically significant negative correlation between vegetation density and the measured LST. Regions characterized by dense vegetation exhibited significantly lower surface temperatures, in stark juxtaposition to urbanized areas where the presence of impervious surfaces contributed to heightened LST values. This scholarly investigation effectively illustrates the indispensable role

that satellite observations and GIS technologies fulfill in the ongoing surveillance of urban thermal dynamics and the complex attributes of land surface characteristics. Furthermore, the study emphasizes the pressing necessity for the implementation of climate-resilient urban planning frameworks, the conservation of green spaces, the augmentation of urban vegetative cover, and the adoption of sustainable land use policies specifically tailored for semi-arid urban environments such as Solapur.

Acknowledgement

Nil.

Financial support and sponsorship

Nil.

Conflicts of interest

The authors declare that there are no conflicts of interest regarding the publication of this paper

References:

1. Chen, M.; Zhou, Y.; Hu, M.; Zhou, Y. Influence of Urban Scale and Urban Expansion on the Urban Heat Island Effect in Metropolitan Areas: Case Study of Beijing–Tianjin–Hebei Urban Agglomeration. *Remote Sens.* 2020, *12*, 3491.
2. Memon, R.A.; Leung, D.Y.C.; Chunho, L. A Review on the Generation, Determination and Mitigation of Urban Heat Island.
3. *J. Environ. Sci.* 2008, *20*, 120–128.
4. Wen, L.J.; Lü, S.H.; Chen, S.Q.; Meng, X.H.; Bao, Y. Numerical Simulation of Cold Island Effect in Jinta Oasis Summer. *Plateau Meteorol.* 2005, *24*, 865–871.
5. Shashua-Bar, L.; Pearlmutter, D.; Erell, E. The Influence of Trees and Grass on Outdoor Thermal Comfort in a Hot-Arid Environment. *Int. J. Climatol.* 2011, *31*, 1498–1506.
6. Rasul, A.; Balzter, H.; Smith, C.; Remedios, J.; Adamu, B.; Sobrino, J.A.; Srivani, M.; Weng, Q. A Review on Remote Sensing of Urban Heat and Cool Islands. *Land* 2017, *6*, 38.
7. Yang, X.; Li, Y.; Luo, Z.; Chan, P.W. The Urban Cool Island Phenomenon in a High-rise High-density City and Its Mechanisms.
8. *Int. J. Climatol.* 2017, *37*, 890–904.
9. Haashemi, S.; Weng, Q.; Darvishi, A.; Alavipanah, S.K. Seasonal Variations of the Surface Urban Heat Island in a Semi-Arid City.
10. *Remote Sens.* 2016, *8*, 352.
11. Maimaitiyiming, M.; Ghulam, A.; Tiyp, T.; Pla, F.; Latorre-Carmona, P.; Halik, Ü.; Sawut, M.; Caetano, M. Effects of Green Space Spatial Pattern on Land Surface Temperature: Implications for Sustainable Urban Planning and Climate Change Adaptation. *ISPRS J. Photogramm. Remote Sens.* 2014, *89*, 59–66.
12. Mirzaei, M.; Verrelst, J.; Arbabi, M.; Shaklabadi, Z.; Lotfizadeh, M. Urban Heat Island Monitoring and Impacts on Citizen's General Health Status in Isfahan Metropolis: A Remote Sensing and Field Survey Approach. *Remote Sens.* 2020, *12*, 1350.
13. Saneinejad, S.; Moonen, P.; Carmeliet, J. Comparative Assessment of Various Heat Island Mitigation Measures. *Builde. Environ.* 2014, *73*, 162–170.
14. Deng, Y.; Wang, S.; Bai, X.; Tian, Y.; Wu, L.; Xiao, J.; Chen, F.; Qian, Q. Relationship among Land Surface Temperature and LUCC, NDVI in Typical Karst Area. *Sci. Rep.* 2018, *8*, 1–12.
15. Bokaie, M.; Zarkesh, M.K.; Arasteh, P.D.; Hosseini, A. Assessment of Urban Heat Island Based on the Relationship between Land Surface Temperature and Land Use/Land Cover in Tehran. *Sustain. Cities Soc.* 2016, *23*, 94–104.
16. Zhou, W.; Huang, G.; Cadenasso, M.L. Does Spatial Configuration Matter? Understanding the Effects of Land Cover Pattern on Land Surface Temperature in Urban Landscapes. *Landsc. Urban Plan.* 2011, *102*, 54–63.
17. Weng, Q.; Liu, H.; Liang, B.; Lu, D. The Spatial Variations of Urban Land Surface Temperatures: Pertinent Factors, Zoning Effect, and Seasonal Variability. *IEEE J. Sel. Top. Appl. Earth Obs. Remote Sens.* 2008, *1*, 154–166.
18. Mallick, J.; Kant, Y.; Bharath, B.D. Estimation of Land Surface Temperature over Delhi Using Landsat-7 ETM+. *J. Ind Geophys Union* 2008, *12*, 131–140.
19. Zhibin, R.; Haifeng, Z.; Xingyuan, H.; Dan, Z.; Xingyang, Y. Estimation of the Relationship between Urban Vegetation Configuration and Land Surface Temperature with Remote Sensing. *J. Indian Soc. Remote Sens.* 2015, *43*, 89–100.
20. Rotem-Mindali, O.; Michael, Y.; Helman, D.; Lensky, I.M. The Role of Local Land-Use on the Urban Heat Island Effect of Tel Aviv as Assessed from Satellite Remote Sensing. *Appl. Geogr.* 2015, *56*, 145–153.
21. Guo, G.; Zhou, X.; Wu, Z.; Xiao, R.; Chen, Y. Characterizing the Impact of Urban Morphology Heterogeneity on Land Surface Temperature in Guangzhou, China. *Environ. Model. Softw.* 2016, *84*, 427–439.
22. Abutaleb, K.; Ngie, A.; Darwish, A.; Ahmed, M.; Arafat, S.; Ahmed, F. Assessment of Urban Heat Island Using Remotely Sensed Imagery over Greater Cairo, Egypt. *Adv. Remote Sens.* 2015, *4*, 35.
23. Bakarman, M.A.; Chang, J.D. The Influence of Height/Width Ratio on Urban Heat Island in Hot-Arid Climates. *Procedia Eng.* 2015, *118*, 101–108.
24. Schatz, J.; Kucharik, C.J. Seasonality of the Urban Heat Island Effect in Madison, Wisconsin. *J. Appl. Meteorol. Climatol.* 2014, *53*, 2371–2386.
25. Arnfield, A.J. Two Decades of Urban Climate Research: A Review of Turbulence, Exchanges of Energy and Water, and the Urban Heat Island. *Int. J. Climatol. J. R. Meteorol. Soc.* 2003, *23*, 1–26.
26. R. Bala, R. Prasad, V.P. Yadav, Disaggregation of modis land surface temperature in urban areas using improved thermal sharpening



- techniques, *Adv. Space Res.* 64 (2019) 591–602, <https://doi.org/10.1016/j.asr.2019.05.004>.
30. R. Bala, R. Prasad, V.P. Yadav, Quantification of urban heat intensity with land use/land cover changes using Landsat satellite data over urban landscapes, *Theor. Appl. Climatol.* 145 (2021) 1–12, <https://doi.org/10.21203/rs.3.rs-243576/v1>.
31. A.A. Khan, A. Jamil, D. Hussain, M. Taj, G. Jabeen, M.K. Malik, Machine-learning algorithms for mapping debris-covered glaciers: the Hunza Basin case study, *IEEE Access* 8 (2020), <https://doi.org/10.1109/ACCESS.2020.2965768>, 12725–12734.
32. Pakistan bureau of statistics. District wise census results, Available at: <http://www.pbscensus.gov.pk/sites/default/files/bwpsr/kp/>, 2017. (Accessed 21 March 2022). Accessed on.
33. M. Afzaal, M.A. Haroon, Q. Zaman, Interdecadal oscillations and the warming trend in the area-weighted annual mean temperature of Pakistan, *Pak. J. Meteorol.* 6 (2009) 13–19.
34. A.A. Mohamed, J. Odindi, O. Mutanga, Land surface temperature and emissivity estimation for Urban Heat Island assessment using medium- and low-resolution space-borne sensors: a review, 49, *Geocarto Int.* 60 (2017) 1–16, <https://doi.org/10.1080/10106049.2016.1155657>.
35. D.A. Artis, W.H. Carnahan, Survey of emissivity variability in thermography of urban areas, *Remote Sens. Environ.* 12 (1982) 313–329, [https://doi.org/10.1016/0034-4257\(82\)90043-8](https://doi.org/10.1016/0034-4257(82)90043-8).
36. J.A. Sobrino, J.C. Jimenez-Munoz, L. Paolini, Land surface temperature retrieval from LANDSAT TM 5, *Remote Sens. Environ.* 90 (2004) 434–440, <https://doi.org/10.1016/j.rse.2004.02.003>.
37. [org/10.1016/j.rse.2004.02.003](https://doi.org/10.1016/j.rse.2004.02.003).
38. L. Cao, H.W. Hu, X.L. Meng, J.X. Li, Relationship between land surface temperature and key landscape elements in urban area, *Chinese J. Ecol.* 30 (2011) 2329–2334.
39. J. Wang, P.M. Rich, K.P. Price, Temporal responses of NDVI to precipitation and temperature in the central Great Plains, USA, *Int. J. Rem. Sens.* 24 (2003) 2345–2364, <https://doi.org/10.1080/01431160210154812>.
40. K.E. Frey, L.C. Smith, How well do we know northern land cover? Comparison of four global vegetation and wetland products with a new ground-truth database for West Siberia, *Global Biogeochem. Cycles* (2007) 21, <https://doi.org/10.1029/2006GB002706>.
41. G. Mieke, S. Mieke, J. Vogel, D. La, Highest treeline in the northern hemisphere found in southern Tibet, *Mt. Res. Dev.* 27 (2007) 169–173, <https://doi.org/10.1659/mrd.0792>.
42. C. Hoorn, A. Perrigo, A. Antonelli, *Mountains, Climate and Biodiversity*, John Wiley & Sons, 2018.
43. H. Phan, F. Andreotti, N. Cooray, O.Y. Che'n, M. De Vos, Joint classification and prediction CNN framework for automatic sleep stage classification, *IEEE Trans. Biomed. Eng.* 66 (2018) 1285–1296, <https://doi.org/10.1109/TBME.2018.2872652>.
44. T.A. Akbar, Q.K. Hassan, S. Ishaq, M. Batool, H.J. Butt, H. Jabbar, Investigative spatial distribution and modelling of existing and future urban land changes and its impact on urbanization and economy, *Rem. Sens.* 11 (2019) 105, <https://doi.org/10.3390/rs11020105>.
45. U. Schickhoff, The upper timberline in the Himalayas, Hindu Kush and Karakorum: a review of geographical and ecological aspects, 275, in: *Mountain Ecosystems*, Springer, Berlin, Heidelberg, 2005, p. 354, https://doi.org/10.1007/3-540-27365-4_12.
46. Z. Qin, A. Karnieli, P. Berliner, A mono-window algorithm for retrieving land surface temperature from Landsat TM data and its application to the Israel-Egypt border region, *Int. J. Rem. Sens.* 2 (2001) 3719–3746, <https://doi.org/10.1080/01431160010006971>.
47. J.C. Jimenez-Munoz, J.A. Sobrino, A generalized single-channel method for retrieving land surface temperature from remote sensing data, *J. Geophys. Res. Atmos. (D22)* (2003), 1082003, <https://doi.org/10.1029/2003JD003480>.
48. Q. Fu, K.N. Liou, On the correlated k-distribution method for radiative transfer in nonhomogeneous atmospheres, *J. Atmos. Sci.* 49 (1992) 2139–2156, [https://doi.org/10.1175/1520-0469\(1992\)049%3C2139:OTCDMF%3E2.0.CO](https://doi.org/10.1175/1520-0469(1992)049%3C2139:OTCDMF%3E2.0.CO).
49. Z. Kan, C. Liu, Z. Li, Retrieval of land surface temperature based on Landsat-8 thermal infrared data and heat island effect analysis over the Taihu Lake region, *J. East China Normal Univ. (Nat. Sci.)* 4 (2016) 129–138, <https://doi.org/10.1007/s40333-014-0071-z>.
51. P. Feng, H. Yue, X. Liu, Land surface temperature inversion based on Landsat 8 data: take the main city of Harin as an example, *Geomat. Spat. Inf. Technol.* 41 (2018) 223–225, <https://doi.org/10.1038/s41598-020-67423-6>.
52. J.A. Sobrino, N. Raissouni, Z. Li, A comparative study of land surface emissivity retrieval from



- NOAA data, *Remote Sens. Environ.* 75 (2001) 256–266, [https://doi.org/10.1016/S0034-4257\(00\)00171-1](https://doi.org/10.1016/S0034-4257(00)00171-1).
53. E. Valor, V. Caselles, Mapping land surface emissivity from NDVI: application to European, African, and South American areas, *Remote Sens. Environ.* 57 (1996) 167–184, [https://doi.org/10.1016/0034-4257\(96\)00039-9](https://doi.org/10.1016/0034-4257(96)00039-9).
54. Z. Qin, W. Li, B. Xu, Z. Chen, J. Liu, Te estimation of land surface emissivity for Landsat TM6, *Remote Sens. Land Resour.* 28 (2004) 36–41, <https://doi.org/10.1117/12.689310>.
55. L.G. Ahmad, A.T. Eshlaghy, A. Poorebrahimi, M. Ebrahimi, A.R. Razavi, Using three machine learning techniques for predicting breast cancer recurrence,
56. *J. Health Med. Inf.* 4 (2013) 3, <https://doi.org/10.4172/2157-7420.1000124>.
57. V.N. Vapnik, An overview of statistical learning theory, *IEEE Trans. Neural Network.* 10 (1999) 988–999, <https://doi.org/10.1109/72.788640>.
58. Y. Deng, S. Wang, X. Bai, Y. Tian, L. Wu, J. Xiao, Q. Qian, Relationship among land surface temperature and LUCC, NDVI in typical karst area, *Sci. Rep.* 8 (2018) 1–12, <https://doi.org/10.1038/s41598-017-19088-x>.
59. M.W. Kilpatrick, N.I.C.M. Artinez, J.P. Little, M.E. Jung, A.M. Jones, N.W. Price, D.H. Lende, Impact of high-intensity interval duration on perceived exertion, *Remote Sens. Environ.* 165 (2015) 1038–1046